Journal of Optics
https://doi.org/10.1007/s12596-024-01794-1

RESEARCH ARTICLE

Highly Efficient Refractive Index Sensor Of Multiple Fano-Resonances Simulated By Polarization-Insensitive Meta-Surface With Silver Nanorings

Khizzra Aslam[1] · Nouraiz Mushtaq[2] · Guoguo Kang[1]

Received: 2 October 2023 / Accepted: 8 March 2024

Abstract
An optical refractive index(RI)sensor is a sensing equipment that can alter variations in the RI into measurable optical data. The grouping of surface plasmon resonance (SPR) and Fano resonance can enhance some key parameters, which are all linked to the complete performance for highly-precise and multi-band sensor. This study purposes and analyze Fabry–Perot (F-P) cavity for optical RI sensing based on the critical coupling condition, effective in a near-infrared (NIR) wavelength range. The simulation shows that the proposed meta-surface exhibits double Fano-resonance by the coupling of the confined surface plasmon resonances (LSPR) of the NR array and the cavity mode of the F-P resonant cavity, at the wavelength of 785 and 1064 nm for an aqueous background medium surrounding the metasurface. Some important optical indexes, polarization sensitivity, figure of merit (FOM) and sensing sensitivity can be improved by the grouping of surface plasmon resonance (SPR) and Fano resonance which are entirely associated to the wide-ranging performance for excellent accuracy and multi-band detecting. Proposed simulation results shows that the excellent sensing sensitivities can attain 650 nm/RIU and 1001.5 nm/RIU, and the corresponding FOMs can significantly attain 226.48 and 247.89. Then we considered the effect of the structural limitations on the sensitivity and FOM of the sensor by simulations and confirmed the structure is in-sensitive to the polarization angle of incident light. Our sensor has excellent performance in polarization insensitivity, good sensing sensitivity and FOM in both resonance bands, which is further appropriate for applied applications.

Keywords Refractive index sensor · Surface plasmon resonance · Meta-surface · Nanoarray · Fano resonance

Introduction

Sensing techniques has been advanced in many areas to vary the limited space and sensitivity of human intelligences. Between the diversity of sensors, RI sensors are extensively used in environmental surveillance, bioanalytic, medical diagnostics, and material recognition etc. To exactly distinguish and precisely analyze several liquids and gases, there have been various optical resonance assemblies used, like FP interferometers, GMR structures, SPP resonance structures, Fano resonance structures, Tamm plasmon (TP) resonance structures and bound states in the continuum (BIC) structures. On the basis of these resonance structures, the RI sensors sense the change in a dip location (λ_0) or resonance peak along the optical band by changing background medium. To attain a highly precise RI sensor, $\Delta\lambda_0$ should be sufficiently large to determine and to calculate the signal with good sensitivity. Optical Refractive index sensor has many applications in biological science, since the concertation of cancerous cells as well as the assault of viruses are frequently convoyed through variations in RI statistically [1]. Plasmonic RI sensor is a type of optical sensor fabricated on the metallic nanostructures which are widely used [2–4]. Amongst them, SPR based sensing [5, 6] is a progressive method and most practically used in industrial applications. An advance improvement in a LSPR based sensing

✉ Khizzra Aslam
khizzraa@yahoo.com

[1] School of Optics and Photonics, Beijing Institute of Technology, Beijing 10081, China

[2] School of Material Science and Engineering, Zhejiang Sci-Tech University, Hangzhou, China

Published online: 21 March 2024

[7] which frequently happens in precious metallic particles, and its reverberation frequency peak is associated to the structural parameters and change in a RI of the background medium, thus, the RI changes will source the change of the LSPR peak and sensing ability.

Nanomaterial structural parameters and material composition greatly affects the LSPRs features as well as EM near-field distributions in addition to positioning of particles, incident angle of source, photon wavelengths, and background medium [8–10]. The presence of LSPRs can localized and manipulated the incident photon in course of matter-photon interaction. Nanostructures of metals which are extensively used because of their ability to improve local electromagnetic fields as well as field detention. Even though noble metal NP of different structural parameters have been considered comprehensively with restricted tunability, plasmonic nanostructures such as reduced NPs, hollow NPs, nanocage NPs, core–shell NPs and nanorings (NR), in precise, exposed up an innovative and important method of guidance of LSPRs reliant on their sizes and topographical characteristics [11–15]. Among several plasmonic nanostructures, noble metal NRs have gain huge attention due to some admirable characteristics. NRs of noble metals provides us with plasmonic resonances in the extensive array of wavelengths with visible, infrared (IR) and near-infrared (NIR) range dependent on their normal thickness, width and the proportion between internal and external rings [16–18]. NRs facilities LSPRs-arbitrated EM near-field disseminations were described to be confined at internal and external shells depending on the incident wavelengths [19, 20]. These plasmonic features form flexible parts with geometry-based responses and have several required properties, for example the chance to restrict light to sub-wavelength parameters and huge local field enrichments. Metals also have inherent nonlinear optical factors that are several orders of size greater than dielectric materials [21].

Nanoparticle polarization by an incident light is dependent on its structure, performing as a loss preventing dipole wire and containing light for a short interval. In comparison of photonic sensors, dipoles resonance can be access simply in metasurface through a beam of light in permitted space as well as a sub-wavelength proliferation area is just needed for resonant operation. Hence, a resonating plasmonic metasurface allows a sequence of specified optical results, comprising optical resonance effects by nonlinear phase-matching, multi-mode process, spatially localized optical response and an intensely localized field enhancement. These metasurfaces by a high-quality factor (Q-factor) might be utilized as a void for applications that requires enlarged light–matter exchanges, high enhanced field, huge optical nonlinearities and small mode volumes, for example an absolutely flat nano-laser with a frequency transformation applications or high transverse mode size [4, 19].

In comparison of previous methods using natural materials, metasurface-based sensors exhibit smaller volumes and have been simulated by many methods. Its precise responses are attained by designing modified periodic arrays of sub-wavelength resonators to modulate the characteristics of electromagnetic wave broadness, transmission direction, phase and polarization. At mean time, the respond of metasurface strongly relies on the RI of the environment. 2D materials composed of nanostructures are also defined as Meta-surfaces. Because of its ultra-rigid size and distinctive photosensitive properties, it has fascinated many academics [22–26]. These nanostructures of meta-surfaces can create LSPR, and the RI of the related medium affects the resonant frequency. Meta-surface could be deliberated as LSPR refractive index sensor, for example nanoring, nanodisk and H-shape metasurfaces respectively [27–29]. High ohmic drop of the metal configuration in LSPR-based meta-surface creates high sensitivity and large value of full width and half maximum (FWHM) at the resonant peak. If the FWHM at the resonant peak has high value resulting a low figure of merit (FOM). In literature the H-shape metasurface having sensing sensitivity with high value, nevertheless its FOM is merely low [27]. This will be cause of the resonance peak shift which is challenging to differentiate in applied methods and disturb the sensing behavior.

Fano resonance produced through the combination of illuminated state and dark state could be utilized to advance the sensing behavior because of its fine irregular resonance line spectral profile [30]. The intensely confined electric fields can significantly increase the interaction among the light and substances. Thus, Fano resonances are extensively used to design highly efficient sensors in various structural systems, such as coupled graphene systems, metamaterials, metallic and dielectric metasurface and metal-dielectric-metal waveguides, coupled and so on. The metal and dielectric hybrid surface will increase the sensitivity of the sensor based on Fano resonances because of the highly optical field binding characteristics of SPs. Furthermore, as compared to the metallic metamaterials, ultra-narrow spectra of the Fano resonance can be recognized in the metal and dielectric hybrid metamaterials. By using metal and dielectric as a hybrid material on a glass substrate enhanced the Fano resonance effect due to its strong coupling and shows narrow resonance peak.

Its narrow resonance peak signifies a minor FWHM consistent to a large sensing FOM. F For instance, the metasurface can realize dual-band sensing by using asymmetric double metallic nanotriangles [31–35] and the irregular metasurface self-possessed of nanorings as well as nanodisks may comprehend tri-band detection [36], mutually they can

accomplish great sensing sensitivity. Hence, utmost Fano resonances have been produced by the destructive coupling of irregular arrangements. Even though the enhanced FOM of sensing are limited by the precise states of the divergence of the incident light. To summarize, FOM, the polarization sensitivity and sensing sensitivity are entirely vital for a device, particularly for good accuracy, accuracy and multi-band detection. Hence, a sensor with good optical result and comprehensive behavior is extremely desired. Related with metamaterials, metasurface is a novel kind of two-dimensional simulated nanostructure, which is of low damage, convenient fabrication, and has benefits in adjusting light in nanoscale, so it has significant value in the field of optical devices. Consequently, illuminating the generation and performing mechanism of the Fano-resonance in an easy fabricated metasurface, and exploring sensing developments may perform a significant part in designing ultra-high sensitivity nano-sensors.

In this work, we simulated a meta-surface self-possessed of an F-P resonant cavity and a hybrid substrate used for RI sensor. It is anticipated to acquire the dual Fano resonances concluded the connection of the LSPR of the NR array and the cavity mode of the F-P resonant cavity. We will observe the effect of the structural parameters on the sensitivity of sensor and FOM with simulation study and examine the polarization sensing sensitivity according to the altering polarization state of the incident light.

Theory

The simulation is based on a meta-surface with NR arrangement as well as F-P resonant cavity. The resonant state of a predictable F-P cavity through of dual reflecting glasses happens when the circular optical phase in the cavity is a numeral time of 2π. This inflicts a restriction on the hollow thickness to gather the desired phase. Our method to overwhelmed this restriction is to dwelling a high dielectric material in the two glasses which persuades a solid phase change and recompenses for the compact accrued phase in the respite of the hollow structure. The LSPR by Nano rings can be easily generated by an incident plane wave which shows an extensive resonance peak. It might be utilized like a bright form that produces Fano resonance. To give the cavity approach with a thin resonance, peak the F-P resonant cavity could be secondarily enthusiastic through the striking radiation. These peaks can be utilized as a dim mode which produces Fano resonance. Hence, through interchanging the metallic film with a NR array at the upper of the F-P resonant cavity, the Fano resonance could produce through the combination of the illuminated as well as lightless state. Descriptions about sensitivity and FOM are given below [37],

$$\mathrm{S} = \Delta\lambda/\Delta\mathrm{n} \tag{1}$$

$$\mathrm{FOM} = \mathrm{S}/\mathrm{FWHM} \tag{2}$$

here Δλ agrees to the variations in the reverberating wavelength as the RI of the background environment deviations Δn, and FWHM signifies the complete thickness of the resonant peak at half maximum. In demand to enhance the sensor execution from the two perceptions of the F-P resonant cavity and NR array, we will hypothetically study the effect of the structural specifications on the FOM and sensitivity.

Toward the F-P resonant cavity, the cavity length L of the resonant cavity has been associated to the resonance wavelength λ_N of the N-order cavity mode, and the connection amongst them which is given below [38].

$$\lambda_N = 2n_T\left(L + \delta\right)/N \tag{3}$$

Where n_L is an adjustable signifying the RI of the background environment in the cavity, δ is a constant. Shown in Eq. 3.

$$\lambda_N/n_L = 2\left(L + \delta\right)/N \tag{4}$$

Sensitivity defines the variations inside a resonance wavelength consistent to the change in unit RI. We can see from Eq. 4 that cavity length and N-order cavity which is linked to the relation of the reverberation wavelength to the RI in the cavity, then we derived an Eq. (5)

$$\mathrm{S} \sim 2\left(L + \delta\right)/N \tag{5}$$

Equation (5) represents that the sensor sensitivity is linked to the cavity mode order N and the cavity length L. The NR arrangement contributes in the connection as a resonant mode with large restraining which links with a huge FWHM. We will further observe the effect of the FWHM of the reflection band produced through the NR on the performance of the sensor. The spectral form of Fano resonant peak has been described through q which represents Fano parameter in the characteristic of Fano eq.

$$\sigma\left(E\right) = D^2(q + \Omega)^2/1 + \Omega \tag{6}$$

Here energy is denoted by E, $D^2 = 4\sin^2\delta$, δ is the change in point of the range. $\Omega = 2(E - E_0)/\Gamma$, where E_0 and Γ are the resonance energy and width, correspondingly. When the resonance mode with excessive restraining γe as well as the

resonance condition with minor damping γ_o are joined, the spreading spectra of Fano resonance is shown below [39].

$$T = [T_0(\omega - \omega_0 + q\gamma_o)^2/(\omega - \omega_0)^2 + \gamma^2{}_o] + T_b \quad (7)$$

here Tb is the related parameter, ω_0 is the resonance frequency, while $q = c_o\gamma_e/[c_e(\omega_{0e} - \omega_{0o})]$, co and c_e are physical numerals, ω_{0e} and ω_{0o} are the resonance frequencies of the dual resonance states. From the eq. of q, we may observe that the q is linked to the frequency alteration among the dual resonance modes and the damping constant γ_e. When $\omega_{0e} - \omega_{0o}$ does not vary, we can perceive that the alteration of γ_e will affect the Fano parameter q, thus altering the spectral form of Fano resonance, so the FWHM of the Fano resonance will also vary, which in result effects the sensing FOM.

Results and discussions

The proposed sensor is simulated by using finite-difference time-domain (FDTD) [40]. Moreover, we choose silver for metal material whose dielectric constant has a minor positive imaginary quantity and a negative real quantity, it can strengthen resonance of Localized surface plasmon polaritons (SPPs) in the deliberated NIR [41]. The unit structure comprises of a single ring stimulated on a hybrid substrate. Hybrid substrate is composed of silver film and dielectric material ($n = 2.93$) on a glass (SiO_2) substrate. Mesh size is 2 nm of our defined structure. The used confine conditions are periodic in both xy-directions and the PML (Perfect matched layer) is in z-direction. Periodic boundary conditions permit the periodic unit structure in xy-directions [42]. Hence electric field enhancement, transmission spectrum and reflection spectrum are attained through frequency-domain area and control monitors. Our purposed sensor is shown below in Fig. 1 which consists of nanoring array with a SiO_2 substrate. The outer radii R and inner radii r of the NR are 130 and 60 nm, correspondingly, the width of Ag substrate is 70 nm and dielectric layer is 55 nm, the nanoring periodic array is used such as $P_x = P_y = 300$ nm, and the surrounding RI of the sensor is an aqueous medium. The perpendicular plane wave whose polarization route is with the y-direction is projected on the sensor. There is a F-P resonant cavity which is a cooperated with dual silver films having a width of 50 nm in Fig. 1b, there is 790 nm cavity length L between two silver films, while SiO_2 is used as a substrate, and the background medium in a cavity is an aqueous solution.

We simulated another structure which is exhibited in Fig. 1c by interchanging the upper silver layer of the F-P resonant cavity having the NR arrangement, and the consistent reflection band of this structure is exhibited in Fig. 1g. We also observe, the NR array has a dual resonance peak at a 701 and 1006 nm resonant wavelength. The gap difference between dual band resonance peak is lower than the reflection spectra of the F-P cavity by using hybrid substrate is exhibited in Fig. 1e. We could observe two fine resonance peaks at the wavelengths of 785 as well as 1064 nm. Electric field enhancements showed that there are two resonance wavelengths in the inset of electric field distribution. The nanocavity consist of two silver films as reflecting outsides,

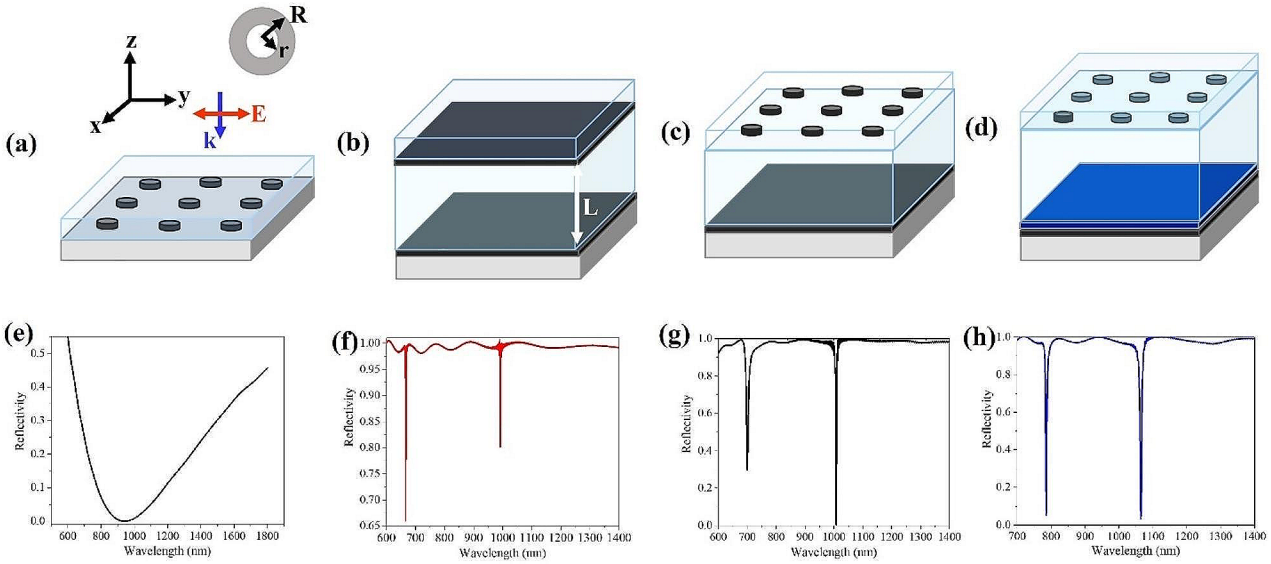

Fig. 1 Scheme of the (**a**) NR array (**b**) F-P resonator (**c**) F-P resonant cavity (**d**) our structure (**e**) Transmission spectrum of NR array (**f-h**) reflectance spectra of the F-P resonator, F-P resonant cavity and our structure (**e**) the intracavity electric field at wavelengths 785 and 1028 nm (**f**) the intracavity electric field at wavelengths 785 and 1064 nm

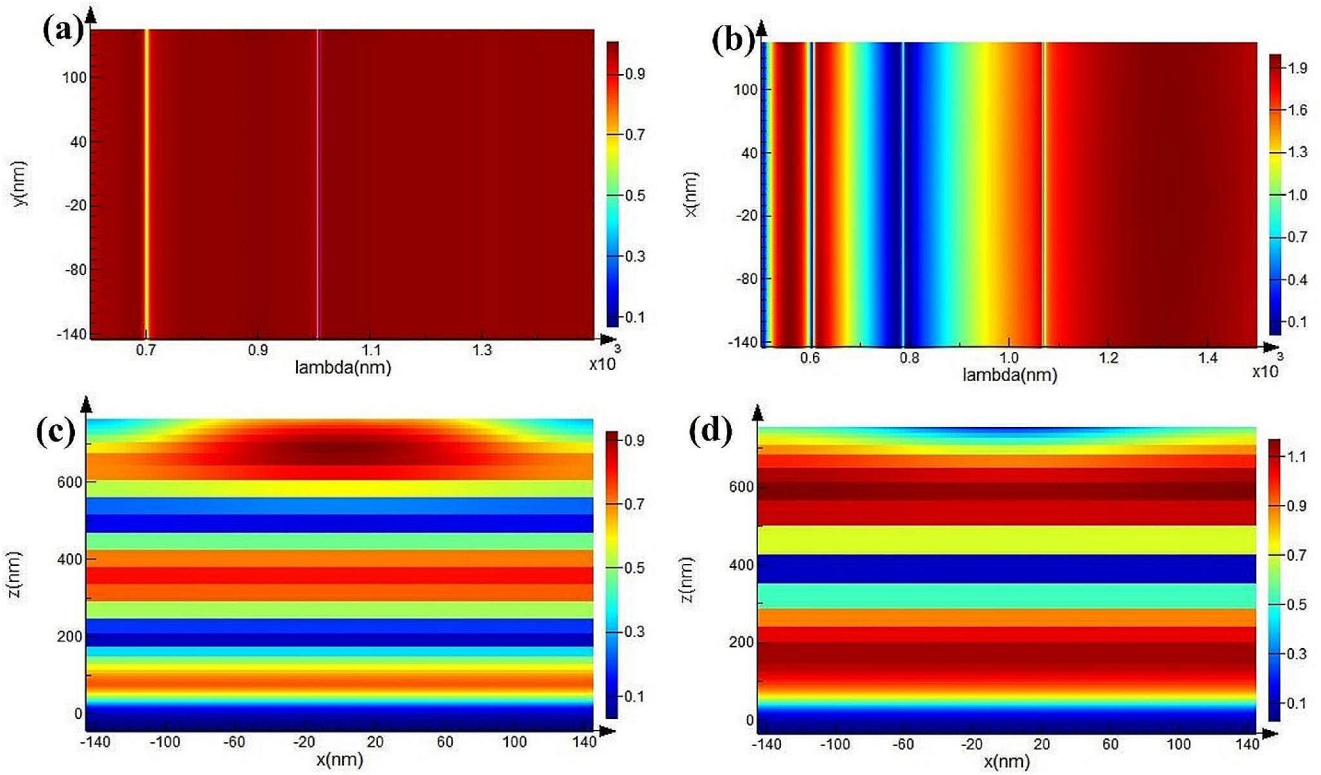

Fig. 2 The electric field at resonance wavelengths for (**a**) F-P resonant cavity (**b**) simulated structure (**c**) The resultant intra-cavity electric field at resonance wavelengths (**c**) 785 nm (**d**) 1064 nm

an Ag-based NR metasurface detached from the lower Ag mirror through a dielectric spacer film, and an aqueous medium which fill out the remaining cavity. Two fine resonance peaks are observed at the resonant wavelengths of 785 and 1064 nm which show Fano-resonances produced with the combination of the illuminated and the dark condition. In this study the illuminated state is the resonance refers to the LSPR of the NR array which are directly excited by incident plane wave. The dark condition is a resonance that raises the reverberation of the F-P cavity secondarily excited in incident light.

The Fig. 2a and b illustrates the E.F at both resonance wavelengths, so we can observe that they relate to the connection of the cavity means respectively. Figure 2c and d shows the relative intra-cavity E.F at 785 and 1064 nm resonance wavelengths, so we can perceive that they match to the coupling of the third-order and second-order cavity modes, correspondingly. So, it is justifying that there is an influence of the F-P cavity to Fano resonances. The support of LSPR to Fano resonances can be demonstrated through the study of electromagnetic domain. Our suggested composition can give two peaks of Fano resonance having a fine resonance line form, which builds the groundwork for its utilization as a sensor.

Metasurface arrangements can excite resonances at any preferred frequency dependent on their fundamental parameters, and these resonances strongly affected by the change in the effective RI of the substrate or surface. Consequently, it is essential to examine the influence of the RI changes in the cavity medium. Therefore, we studied the Fano-resonance effect, sensitivity as well as FOM of the assembly by changing the RI (n_c) of cavity medium. We simulated the structure by using five cavity mediums with RI of 1.31, 1.33, 1.35, 1.37, and 1.39. The relevant reflection graph by changing refractive index of cavity media is shown in Fig. 3(b). Increase in the RI of cavity media displays significant redshift in the resonant wavelength. The corresponding sensitivities of right and left resonant peaks are 1001.5 nm/RIU and 650 nm/RIU and the full width half maximum consistent with the right and left peaks are around 4.0 and 2.87 nm, respectively as see in the Fig. 3(b). The calculated FOMs of the double peaks are 247.89 and 226.48, correspondingly. The dual Fano resonances with ultra-thin resonant peaks [43] has been demonstrated that varying the aqueous medium to $Si0_0$ and inserting the analyte medium on the upper side of the NR array, consequently it is compulsory to examine both sensitivity and FOM of this analyte medium structure underneath the similar circumstances. The analyte medium structure and the relevant reflection

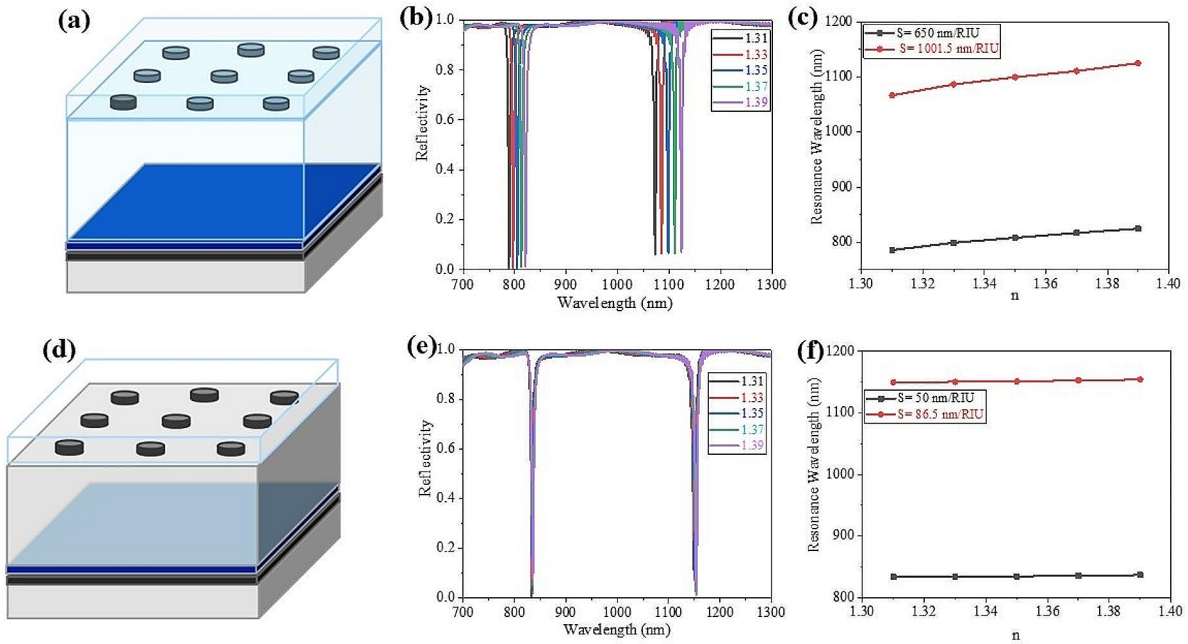

Fig. 3 Schematic illustration of the tested medium (**a**) the upper side of the geometry (**d**) in the cavity (**b, e**) reflection spectrum when the RI are 1.31, 1.33, 1.35,1.37 and 1.39. (**c, f**) sensitivities

spectra by changing the RI of the medium on the upper side of the structure are observed in Fig. 3(d) and 3(e). We can observe that, there is essentially no change in resonance wavelengths as the RI increases and the curves of resonance peaks practically overlap. The FWHMs of the right and left peaks are 5.2 nm and 4.8 nm, and the sensitivities of the dual-band peaks are around 86.5 nm/RIU and 50 nm/RIU, respectively, and then further estimated FOMs approximately about 16.63 and 10.41. Relatively, we observed that when the analyte medium is located between the nanoring array and cavity, the sensitivity and FOM of the structure is considerably advanced apart from the positioned on the upper side of the structure. The RI changes generally affects the resonant peaks by placing analyte medium on the surface of the structure. Minor variations are observed in the Fano resonance because the scheme of cavity remains same so it shows slight impact on the F-P resonant cavity. The wavelengths of Fano resonance have a prominent redshift by the alteration of RI in the test cavity media and will impact together on the resonances of the NR sequence and the cavity of F-P resonant. This summary of our simulated result is reliable with previous study [44].

We primarily considered the designed structure in the following study when the investigated channel is in the cavity because it shows high sensitivity. At that time, we considered the effect of operational parameters by simulation calculation on the FOM and sensitivity the structure. We mostly considered the impact of N and L towards the F-P resonance cavity. From Eq. (5), we observed that the sensor's sensitivity of the F-P resonant cavity structure has been associated to the cavity length as well as mode order L and N, respectively. Noticeable Fano resonances could be created after L is 690, 790 or 890 nm [45]. As L is 690, 790 and 890 nm, then other factors stay unaffected, the resultant reflection spectrum of varying RI are exhibited in Fig. 4(a, b, c). Connection of 4th, 3rd and 2nd order cavity means produced three Fano resonance peaks in the data from left to right. The sensitivity of the three Fano resonance peaks after the cavity length changed shown in Fig. 4 (d, e, f). Over the evaluation, we may observe that the compassion of the resonant peak created through the link of the cavity means of the similar direction becomes high with the rise of the length of cavity, and as the cavity span is continuous, the higher Fano resonance sensitivity is resultant of inferior the directive of the cavity mode contributing in the connection. These outcomes are agreeing with the significance of our proposed Eq. (5). So, the sensitivity can be improved by increasing L and decreasing N.

After that we further investigated the effect of the structural constraints on the NR array sensor. From the Eq. (7), we observed that the FOM of the sensing will get affected by the restraining of NR array. The resonance of nanoring array

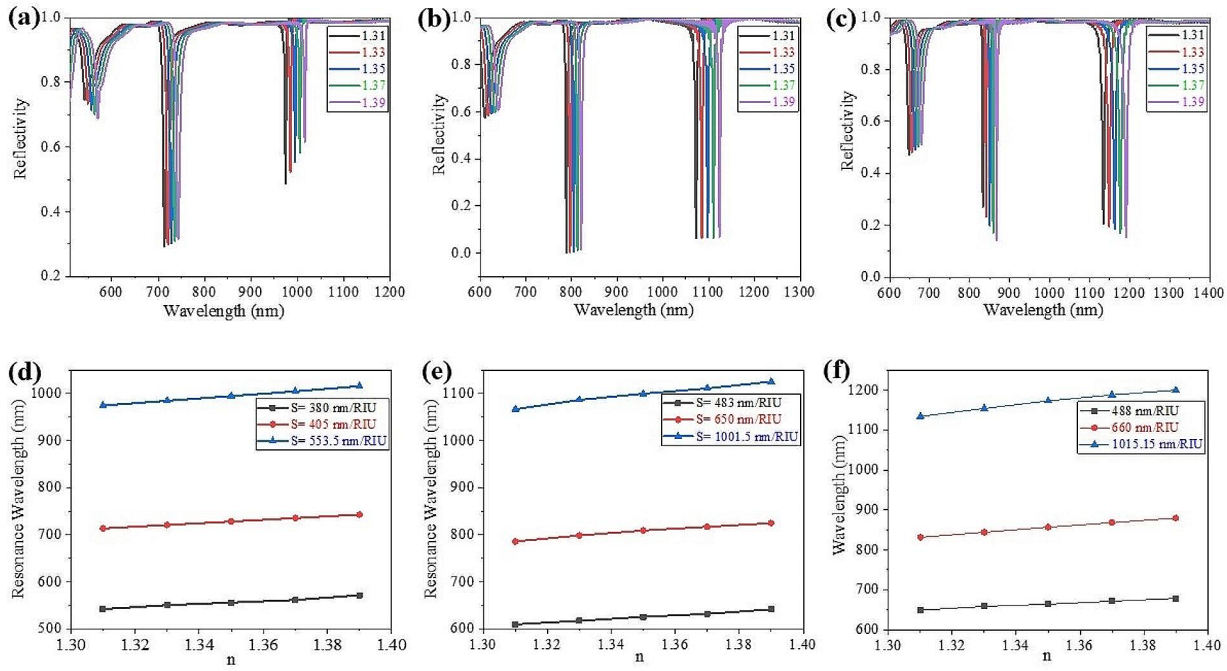

Fig. 4 Reflectance spectra of changed RI when the length L of cavity is (**a**) 690 nm (**b**) 790 nm (**c**) 890 nm (**d-f**) sensitivity of the peaks

is essentially associated to the proportion of the internal and external width of the NR [46]. Then, we enlarged the damping constant via enhancing the external diameter of the NR, thus raising the FWHM of the resonant peak, then on the same interval, set the resonance wavelength continuous in monitoring the internal radius of NR. We regulate the resonance wavelength to around 932 nm by choosing six assemblies of NR arrays with external radii of 140, 130, 120, 110, 100 and 90 nm, and the attuned corresponding internal radii are 60, 62, 61, 63 and 56 nm, correspondingly. The transmittance spectrum of the six assemblies of NR scheme is represented in the brown graphs in Fig. 5(a-f). At that time, we join six assemblies of NR with the F-P resonator and gained the reflectance spectrum when the RI are 1.31, 1.33, 1.35, 1.37, and 1.39, that is signified through the different color graphs in Fig. 4(a-f). We may get that when the transmission of the resonance peak of the NR decreases, the dual Fano resonance peaks go deeper, and similarly FWHMs reduced. The FOM and sensitivity of the resonance peaks are in the Fig. 5(a-f), which are shown in Table 1. We concluded that the sensitivities of the resonance peak a little vary though the FWHM of the transmission spectra of the NR array enhanced whereas the FOMs become considerably higher. These results agree with our hypothetical investigation. Hence, we may realize that the FOM of the sensor compromised of NR can be efficiently enhanced by changing the spectral of the resonance peak. Deeper resonance peak of NR arrangement shows the higher FOM value of the sensor.

Then, we considered the sensitivity of the sensor by varying angle of incident light. The reflection spectra of polarized incident light shown in Fig. 6(a, b). The resonance reflection spectrum of linearly polarized light does not alter as the polarization angles vary from 0 to 180 degrees which are 785 and 1064 nm. When the divergence angle of incident light is LCP as well as RCP, the resonance peak remains unaffected. Consequently, our assembly is unresponsive to the divergence angle of the incident light. It is a most useful structure than the prevailing irregular geometry that produces Fano resonance because it is not limited through the polarization mode of incident light for applied application.

From Fig. 6(c) the FDTD reflectivity spectra with diverse incident light angles that deviate from 0° to 50°. By means of this process for individual incident angle gives us to exactly find out the suitable band and accomplish the part of the F-P resonant cavity. Under normal incidence of light, Fano resonance have a dual band mode on the perceived frequency of reflection peak. The Fano resonance mode damped quickly when incident light mode is introduced by using a larger-order value of based on the angle, on which reflection of the F-P resonant cavity stimulation. These results exhibit that it is feasible to proficiently restraint the spectral significance of the Fano mode resonance, allowing for significant structure cordiality in scheming a sensor. Thus, in the

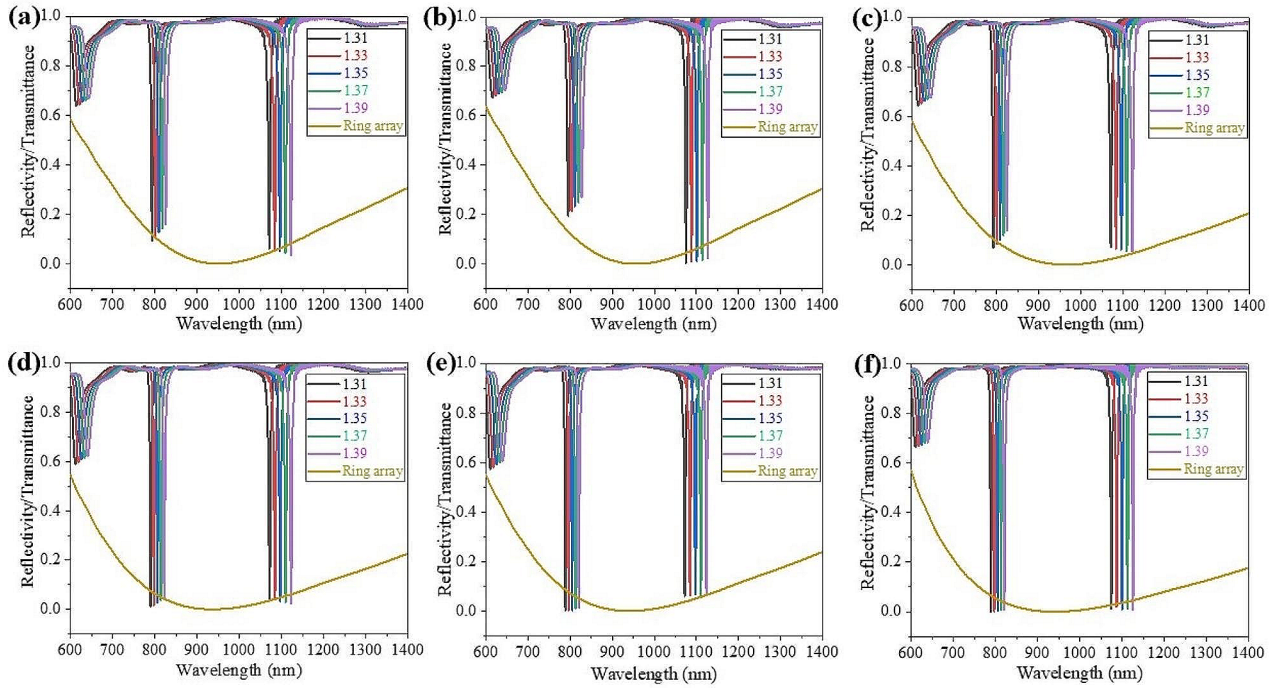

Fig. 5 The transmission spectrum and the reflection spectrum of the NR array with diverse RI of proposed structure with internal and external radii of the NR are (**a**) 90 nm and 56 nm, (**b**) 100 nm and 63 nm, (**c**) 110 nm and 61 nm, (**d**) 120 nm and 62 nm, (**e**) 130 nm and 60 nm, and (**f**) 140 nm and 60 nm

Table 1 FOMs and Sensitivities with different internal and external radii of NR.

Outer radius (nm)	90	100	110	120	130	140
Inner radius (nm)	56	63	61	62	60	60
$FWHM_{(2nd\ Peak)}$	4.41	5.01	3.85	3.45	2.87	3.06
$FWHM_{(3rd\ Peak)}$	4.76	5.31	4.51	4.24	4.0	3.19
2nd Peak S (nm/RIU)	400	410.5	413.5	411	650	418.5
FOM	90.70	81.93	107.40	119.13	226.48	136.76
3rd Peak S (nm/RIU)	600	650	624.5	625	1001.5	649.5
FOM	125.26	122.41	137.51	147.40	247.89	203.605

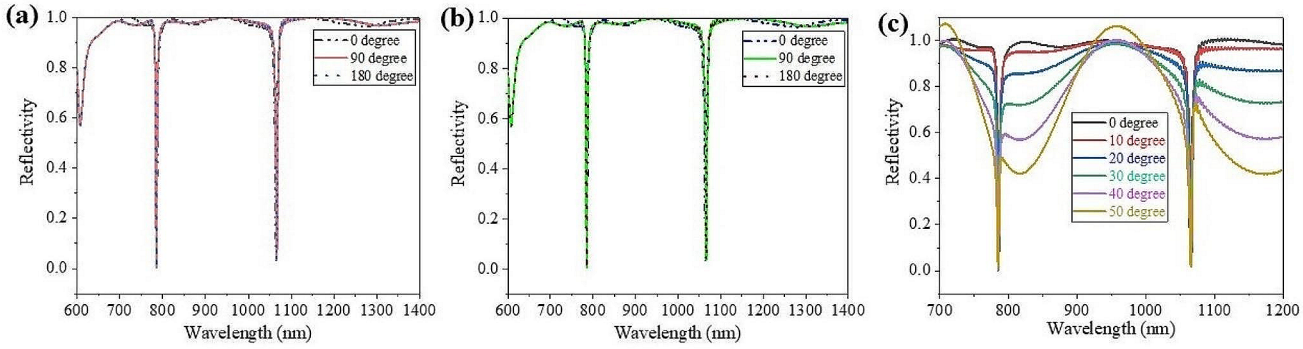

Fig. 6 The reflection spectra of the structure by using (**a**) LCP (**b**) RCP and (**c**) incident angle from 0 to 50 degrees

computation kept $\alpha = 0^{\circ}$ can produce the improved sensing characteristics.

There is a comparison in Table 2 of our sensor with some reported multi-band sensors in means of composition of materials, structural design, sensitivity, FOM, band numeral, and polarization sensitivity. We may conclude that sensors possessed of dual metal micro-cavity, nanotriangles, Dimer Ag rings and nano-bar can attain double-band sensing as well as having advanced sensitivity value, nonetheless they are delicate to the divergence angle of incident light. According to literature, the sensor made of nano-block component and centered-shell nanorods, they are independent of the divergence angle of incident light, then the FOMs values of sensing have been less than 20. The V-shaped probe sensor attained great FOM detection and independent of polarization angle, however the sensing sensitivity value is only reaches up to 186.96 nm/RIU. Four-band detection is recognized in a sensor made of nanodisks with systematic prismatic cavities, while the sensor is polarization-insensitive. These four band sensors have sensitivities of less than 250 nm/RIU and FOMs of smaller than 25. Our purposed sensor can accomplish two resonant peaks in high sensing sensitivity. It also shows large FOMs and independent to the polarization of incident light. Thus, this geometry is harmonized with the desires of an extremely wide-ranging performance sensor.

Conclusions

In the conclusion, we recommended a sensor having multi-band with an extraordinary efficiency. The sensor is fabricated with a silver NR scheme and F-P resonant cavity. The LSPR of the NR and the cavity state of the F-P resonant may be connected to produced dual Fano resonances. The sensitivities of sensor consistent to the dual Fano peaks are 650 nm/RIU and 1001.5 nm/RIU as well as the FOM are 226.48 and 247.89. Then we attained the similar resonance wavelength via altering the divergence of the incident light, which verified that proposed scheme is polarization insensitive. The assessment against reported multi-band RI sensors shows that our proposed sensor has good inclusive activity, and the geometry is reachable with current synthesis methods. The Ag layer and Ag NR can be fabricated on glass substrates separately through lithography and e-beam evaporation method. The cavity can be designed with regulating the gap between the NR metasurface and the Ag layer through piezoelectric transducer, therefore it is further capable to be utilized in drug analysis, ecological monitoring, biosensing and other areas.

Table 2 Evaluation with other multi-band sensors

Materials	Structure	Band number	Sensitivities (nm/RIU)	FOMs (RIU^{-1})	Polarization Sensitivity	Reference
$Ag+SiO_2$	Nanoring cavity	Double-band	650 1001.5	226.48 247.89	Insensitive	This work
Au	double metallic nanotriangles	Double-band	628 362	35 13	Sensitive	[21]
Au	Nano-bar micro-cavity	Double-band	831 638	Not studied	Sensitive	[29]
Ag	Ag rings dimer array	Double-band	470 570	12 21	Sensitive	[36]
Si	Four Holes in Nanoblock Unit	Double-band	306.71 204.27	10.09 16.76	Insensitive	[47]
$Au+SiO_2$	Shell-core nanorods	Double-band	118.232 783.7	2.8 8.2	Insensitive	[48]
TiO_2	V-shaped aerials	Double-band	186.96 184.59	716 721	Insensitive	[37]
Au	Nanodisks with regular prismatic holes	Four-band	249 223 246 119	22.6 15.9 14.9 16.9	Insensitive	[49]
$Au+SiO_2$	Nanoring array cavity	Double-band	693.9 985.6	119.7 119.0	Insensitive	[50]
MIM	Ring shape Metal-insulator-metal	Double-band	567.23 3.72	478.34 2.91		[51]

Supplementary Information The online version contains supplementary material available at https://doi.org/10.1007/s12596-024-01794-1.

References

1. K. Aslam, N. Mushtaq, G. Kang, Z. Luo, Sensing of refractive index by using guided mode resonance 1D TiO_2 grating at visible wavelength under normal incidence. Opt. Rev. **30**, 427–435 (2023)
2. R. Zafar, S. Nawaz, G. Singh, A. D'Alessandro, M. Salim, Plasmonics-based refractive index sensor for detection of Hemoglobin Concentration. IEEE Sens. J. **18**(11), 4372–4377 (2018)
3. A.V. Kabashin, P. Evans, S. Pastkovsky, W. Hendren, G.A. Wurtz, R. Atkinson, R. Pollard, V.A. Podolskiy, A.V. Zayats, Plasmonic nanorod metamaterials for biosensing. Nat. Mater. **8**, 867–871 (2009)
4. A.F. Coskun, A.E. Cetin, B.C. Galarreta, D.A. Alvarez, H. Altug, A. Ozcan, Lens free optofluidic plasmonic sensor for real-time and label-free monitoring of molecular binding events over a wide field-of-view. Sci. Rep. **4**, 6789 (2014)
5. J.F. Masson, Surface Plasmon Resonance Clinical biosensors for Medical Diagnostics. ACS Sens. **2**(1), 16–30 (2017)
6. J. Homola, Surface plasmon resonance sensors for detection of chemical and biological species. Chem. Rev. **108**(2), 462–493 (2008)
7. A. Csaki, O. Stranik, W. Fritzsche, Localized surface plasmon resonance based biosensing. Expert Rev. Mol. Diagn. **18**(3), 279–296 (2018)
8. S. Ma, D. Yang, S. Ding, J. Liu, W. Wang, Z. Wu, X. Liu, L. Zhou, Q. Wang, Tunable size dependence of quantum plasmon of charged gold nanoparticles. Phy Rev. Lett. **126**(17), 173902 (2021)
9. M. Islam, M. Hossen, T. Koschny, Shape and orientation-dependent scattering of isolated gold nanostructures using polarized dark-field microscopy. J. Phys. Chem. C **125**(21), 11478–11488 (2021)
10. T. Tan, C. Tian, Z. Ren, J. Yang, Y. Chen, L. Sun, Z. Li, A. Wu, H. Fu, SPR-dependent SERS performance of silver nanoplates with highly stable and broad tunable LSPRs prepared through an improved seed-mediated strategy. Phys. Chem. Chem. Phys. **15**(48), 21034–21042 (2013)
11. G. Li, C. Cherqui, Y. Wu, N. Bigelow, P. Simmons, P. Rack, D. Masiello, J. Camden, Examining substrate-induced plasmon mode splitting and localization in truncated silver nanospheres with electron energy loss spectroscopy. J. Phys. Chem. Lett. **6**(13), 2569–2576 (2015)
12. N. Zhou, C. Ye, L. Polavarapu, Q. Xu, Controlled preparation of Au/Ag/SnO_2 core–shell nanoparticles using a photochemical method and applications in LSPR based sensing. Nanoscale. **7**(19), 9025–9032 (2015)
13. S. Skrabalak, J. Chen, Y. Sun, X. Lu, L. Au, C. Cobley, Y. Xia, Gold nanocages: synthesis, properties, and applications. Acc. Chem. Res. **41**(12), 1587–1595 (2008)
14. M. Mahmoud, Surface-enhanced Raman spectroscopy of double-shell hollow nanoparticles: electromagnetic and chemical enhancements. Langmuir. **29**(21), 6253–6261 (2013)
15. J. Mokkath, Localized surface plasmon resonances of a metal nanoring. Phys. Chem. Chem. Phys. **22**(41), 23878–23885 (2020)
16. Y. Cai, Y. Li, P. Nordlander, P. Cremer, Fabrication of elliptical nanorings with highly tunable and multiple plasmonic resonances. Nano Lett. **12**(9), 4881–4888 (2012)
17. A. Halpern, R. Corn, Lithographically patterned electrodeposition of gold, silver, and nickel nanoring arrays with widely tunable near-infrared plasmonic resonances. ACS Nano. **7**(2), 1755–1762 (2013)
18. H. Im, K. Bantz, S. Lee, T. Johnson, C. Haynes, S. Oh, Self-assembled plasmonic nanoring cavity arrays for SERS and LSPR biosensing. Adv. Mater. **25**(19), 2678–2685 (2013)
19. W. Lin, Q. Wang, Q. Li, A. Dong, The local surface plasmon resonance property and refractive index sensitivity of metal elliptical nano-ring arrays. AIP Adv. **4**(11), 117115 (2014)
20. C. Huang, J. Ye, S. Wang, T. Stakenborg, L. Lagae, Gold nanoring as a sensitive plasmonic biosensor for on-chip DNA detection. Appl. Phys. Lett. **100**(17), 173114 (2012)
21. J.M. Foley, J.D. Phillips, Normal incidence narrowband transmission filtering capabilities using symmetry protected modes of a subwavelength, dielectric grating. Opt. Lett. **40**(11), 2637–2640 (2015)
22. Y. Lee, S.J. Kim, H. Park, B. Lee, Metamaterials and metasurfaces for Sensor Applications. Sensors. **17**(8), 1726 (2017)
23. D.D. Wen, F.Y. Yue, S. Kumar, Y. Ma, M. Chen, X.M. Ren, P.E. Kremer, B.D. Gerardot, M.R. Taghizadeh, G.S. Buller, X.Z. Chen, Metasurface for characterization of the polarization state of light. Opt. Express. **23**(8), 10272–10281 (2015)
24. P. Mandal, Plasmonic Perfect Absorber for Refractive Index Sensing and SERS. Plasmonics. **11**, 223–229 (2016)
25. S. Naghizade, H. Saghaei, Tunable graphene-on-insulator band-stop filter at the mid-infrared region. Opt. Quantum Electron. **52**, 224 (2020)
26. S.M. Alden Mostaan, H. Saghaei, A tunable broadband graphene-based metamaterial absorber in the far-infrared region. Opt. Quantum Electron. **53**, 96 (2021)
27. P. Mandal, H-Shape Plasmonic Metasurface as Refractive Index Sensor. Plasmonics. **10**, 439–445 (2015)
28. X.Y. Lu, R.G. Wan, T.Y. Zhang, Metal-dielectric-metal based narrow band absorber for sensing applications. Opt. Express. **23**(23), 29842–29847 (2015)
29. N. Liu, M. Mesch, T. Weiss, M. Hentschel, H. Giessen, Infrared Perfect Absorber and its application as Plasmonic Sensor. Nano Lett. **10**(7), 2342–2348 (2010)
30. M.F. Limonov, M.V. Rybin, A.N. Poddubny, Y.S. Kivshar, Fano resonances in photonics. Nat. Photonics. **11**, 543–554 (2017)
31. G.D. Liu, X. Zhai, L.L. Wang, Q. Lin, S.X. Xia, X. Luo, C.J. Zhao, A high-performance refractive index Sensor based on Fano Resonance in Si Split-Ring Metasurface. Plasmonics. **13**, 15–19 (2018)
32. Z.Q. Liu, H.B. Shao, G.Q. Liu, X.S. Liu, H.Q. Zhou, Y. Hu, X.N. Zhang, Z.J. Cai, G. Gu, λ^3/20000 plasmonic nanocavities with multispectral ultra-narrowband absorption for high-quality sensing. Appl. Phys. Lett. **104**(8), 081116 (2014)
33. G.Q. Liu, M.D. Yu, Z.Q. Liu, P.P. Pan, X.S. Liu, S. Huang, Y. Wang, Multi-band High Refractive Index susceptibility of Plasmonic structures with Network-Type Metasurface. Plasmonics. **11**, 677–682 (2016)
34. W. Su, X.Y. Chen, Z. Geng, Y.L. Luo, B.Y. Chen, Multiple Fano resonances in all-dielectric elliptical disk-ring metasurface for high-quality refractive index sensing. Results Phys. **18**, 103340 (2020)
35. Z.D. Yan, X.M. Wen, P. Gu, H. Zhong, P. Zhan, Z. Chen, Z.L. Wang, Double Fano resonances in an individual metallic nanostructure for high sensing sensitivity. Nanotechnology. **28**, 475203 (2017)
36. X.S. Liu, G.L. Fu, X.F. Zhan, Z.Q. Liu, All-metal resonant metamaterials for One-, Two-, three-Band Perfect Light absorbers and sensors. Plasmonics. **14**, 967–971 (2019)
37. H.G. Liu, L. Zheng, P.Z. Ma, Y. Zhong, B. Liu, X.Z. Chen, H.T. Liu, Metasurface generated polarization insensitive Fano resonance for high-performance refractive index sensing. Opt. Express. **27**(9), 13252–13262 (2019)

38. R. Ameling, H. Giessen, Cavity plasmonics: large normal Mode Splitting of Electric and Magnetic Particle Plasmons Induced by a Photonic Microcavity. Nano Lett. **10**(11), 4394–4398 (2010)
39. D.H. Tang, W.Q. Ding, Fano Resonance by Symmetry breaking stub in a metal-dielectric-metal Waveguide. Chin. Phys. Lett. **31**, 057301 (2014)
40. S. Naghizade, H. Saghaei, Tunable electro-optic analog-to-digital converter using graphene nanoshells in photonic crystal ring resonators. J. Opt. Soc. Am. B **38**(7), 2127–2134 (2021)
41. A.A. Tabrizi, H. Saghaei, M.A. Mehranpour, M. Jahangiri, Enhancement of absorption and effectiveness of a Perovskite Thin-Film Solar Cell embedded with Gold Nanospheres. Plasmonics. **16**, 747–760 (2021)
42. M.Z. Tsai, C.T. Hsiung, Y. Chen, C.S. Huang, H.Y. Hsu, P.Y. Hsieh, Real-time CRP detection from whole blood using micropost-embedded microfluidic chip incorporated with label-free biosensor. Analyst. **143**(2), 503–510 (2018)
43. Z.H. Liu, J. Ye, Highly controllable double Fano resonances in plasmonic metasurfaces. Nanoscale. **8**(40), 17665–17674 (2016)
44. Y. Kong, J.J. Cao, W.C. Qian, C. Liu, S.Y. Wang, Multiple Fano Resonance based Optical Refractive Index Sensor composed of Micro-cavity and Micro-structure. IEEE Photonics J. **10**(6), 1–10 (2018)
45. M.Y. Du, Z. Shen, Enhanced and tunable double Fano resonances in plasmonic metasurfaces with nanoring dimers. J. Phys. D Appl. Phys. **14**(54), 145106 (2021)
46. J. Aizpurua, P. Hanarp, D.S. Sutherland, M. Kall, G.W. Bryant, F.J.G. de Abajo, Optical properties of gold nanorings. Phys. Rev. Lett. **90**, 057401 (2003)
47. J. Hu, T.T. Lang, G.H. Shi, Simultaneous measurement of refractive index and temperature based on all-dielectric metasurface. Opt. Express. **25**(13), 15241–15251 (2017)
48. L.L. Shi, Q. Tang, Z.Q. Liu, Y. Liu, Y.Y. Li, G.Q. Liu, L. Li, Tunable dual-band plasmonic perfect absorber and its sensing applications. J. Opt. Soc. Am. B **36**(10), 2750–2756 (2019)
49. L.L. Shi, J.S. Shang, Z.Q. Liu, Y.Y. Li, G.L. Fu, X.S. Liu, P.P. Pan, H.M. Luo, G.Q. Liu, Ultra-narrow multi-band polarization-insensitive plasmonic perfect absorber for sensing. Nanotechnology. **31**(46), 465501 (2020)
50. Z. Shen, M. Du, High-performance refractive index sensing system based on multiple Fano resonances in polarization-insensitive metasurface with nanorings. Opt. Exp. **18**(29), 28287–28296 (2021)
51. Y. Shokorlou, H. Heidarzadeh, H. Bahador, Simulation and Analysis of Ring shape Metal–InsulatorMetal Plasmonic biosensors for the detection of ProstateSpecific Antigen (PSA). Plasmonics. **17**, 2197–2204 (2022)